Biophysical Chemistry 253 (2019) 106216

Contents lists available at ScienceDirect

Biophysical Chemistry

journal homepage: www.elsevier.com/locate/biophyschem

Research Article

Force dependence of unbinding rate of kinesin motor during its processive movement on microtubule

Si-Kao Guo[a,b], Xiao-Xuan Shi[a,b], Peng-Ye Wang[a,b], Ping Xie[a,b,*]

[a] Key Laboratory of Soft Matter Physics, Institute of Physics, Chinese Academy of Science, Beijing 100190, China
[b] School of Physical Sciences, University of Chinese Academy of Sciences, Beijing 100049, China

HIGHLIGHTS

- Force dependence of unbinding rate of kinesin was studied computationally.
- The unbinding rate exhibits slip bond form under forward load.
- The unbinding rate exhibits slip-catch-slip bond form under backward load.
- Mechanism of the slip-catch-slip bond under backward load was revealed.

GRAPHICAL ABSTRACT

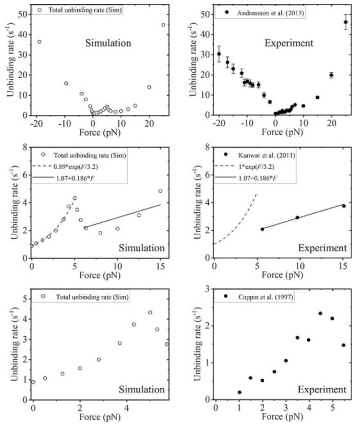

ARTICLE INFO

Keywords:
Kinesin
Dissociation rate
Catch bond
Molecular motor

ABSTRACT

Kinesin is a biological molecular motor that can move continuously on microtubule until it unbinds. Here, we studied computationally the force dependence of the unbinding rate of the motor. Our results showed that while the unbinding rate under the forward load has the expected characteristic of "slip bond", with the unbinding rate increasing monotonically with the increase of the forward load, the unbinding rate under the backward load shows counterintuitive characteristic of "slip-catch-slip bond": as the backward load increases, the unbinding rate increases exponentially firstly, then drops rapidly and then increases again. Our calculated data are in agreement with the available single-molecule data from different research groups. The mechanism of the slip-catch-slip bond was revealed.

1. Introduction

Kinesin is a biological molecular motor that plays a critical role in cargo transport inside cells [1]. It uses the chemical energy of ATP hydrolysis to power its processive movement on microtubule (MT) towards the plus end. To understand the mechanism and dynamics of its processive movement, various methods have been employed in structural biology, biochemical biology, single molecule spectroscopy, molecular dynamics simulation, theoretical modeling, and so on [2–12]. For example, with single-molecule optical trapping methods, the force

* Corresponding author at: Key Laboratory of Soft Matter Physics, Institute of Physics, Chinese Academy of Science, Beijing 100190, China.
E-mail address: pxie@aphy.iphy.ac.cn (P. Xie).

https://doi.org/10.1016/j.bpc.2019.106216
Received 28 May 2019; Received in revised form 26 June 2019; Accepted 30 June 2019
Available online 02 July 2019

dependence of its velocity has been well determined [13–16]. Using theoretical modeling, the simple, analytical form of the force-velocity relation has also been well defined [17,18].

Besides the velocity, the unbinding rate of the kinesin motor during its processive movement on MT is also an important factor to advance our understanding of the motor function. More importantly, to model the collective transport by multiple kinesin/dynein motors, apart from the force dependence of the velocity the force dependence of the unbinding rate of the single motors is also indispensable [19–28]. Based on the Kramers theory, the force dependence of the unbinding rate of the kinesin motor from MT should have an exponential form. However, the experimental evidence of Kunwar et al. [19] indicated that the unbinding rate of the kinesin motor could exhibit a form of "slip-catch-slip bond": as the backward load increases, the unbinding rate increases firstly, then drops rapidly and then increases again. It has been proposed that this non-monotonic behavior is due to the coupling between the detachment and stepping of the motor [29,30] and in particular, it is as a consequence of the consideration that the unbinding rate is proportional to the inverse of the dwell time [30]. In the literature, to study the collective transport by multiple kinesin/dynein motors some works used the exponential unbinding rate for the single kinesin motor [20–25] while others used the slip-catch-slip unbinding rate [19,26,27]. Recently, Dallon et al. [28] studied computationally the transport of intermediate filaments by multiple kinesin and dynein motors using both exponential and slip-catch-slip unbinding rates for the motors, showing that the forms of the unbinding rate have large effects on the collective transport dynamics.

However, whether kinesin motor has an exponential or a slip-catch-slip unbinding rate is still an open question. If the motor has the slip-catch-slip unbinding rate, what is the underlying mechanism? To address these issues, in this work, we study computationally the force dependence of the unbinding rate of the kinesin motor during its processive movement on MT. We use the model presented before that successfully reproduced diverse available single-molecule data on various aspects of the movement dynamics of kinesin motors versus external force of both forward and backward directions [31,32]. Our results on the unbinding rate are in agreement with the available single-molecule data from different research groups. The studies indicate that the dependence of the unbinding rate on the backward load exhibits the exponential form in the small range of the backward load but exhibits slip-catch-slip form in the large range of the backward load. Thus, our work not only is important to the understanding of the functions of the single kinesin motors and to the theoretical and computational studies of the collective transport by multiple kinesin/dynein motors, but also is implicative to the understanding of the mechanism of the slip-catch-slip bond [33].

2. Methods and materials

2.1. The model

To study the force dependence of unbinding rate of kinesin dimer during its processive movement on MT, we use the same model of chemomechanical coupling for kinesin as that presented before to study the force dependence of velocity and processivity (or run length) [31,32]. For convenience of reading, the model is re-described briefly here. The model is built up based mainly on the following pieces of experimental and computational evidence and/or arguments.

(i) A kinesin head in nucleotide-free (φ), ATP or ADP.Pi state has a strong interaction with MT, while in ADP state has a weak interaction [34–36]. The available structural data showed that the strong interaction of kinesin head with MT-tubulin induces large conformational changes in the MT-tubulin [37]. As all-atom molecular dynamics indicated, the large conformational changes result in the local MT-tubulin having a further weaker interaction with the ADP-head than other unperturbed MT-tubulins [38], with the binding energy of ADP-head to the local MT-tubulin (denoted by E_{w1}) being smaller than that to other unperturbed MT-tubulin (denoted by E_{w2}). Since the weak interaction cannot induce conformational changes of MT, in a time of t_r (in the order of μs) after Pi releases from the kinesin head the local MT-tubulin restores to its normally unperturbed conformation, with the binding energy of the ADP-head to the local MT-tubulin becoming E_{w2}.

(ii) For a MT-bound head, in ATP or ADP.Pi state its neck linker (NL) can dock into its motor domain, with a small docking energy (denoted by E_{NL}) and a docking rate (denoted by k_{NL}) in ADP.Pi state being much larger than that in ATP state, whereas in φ or ADP state the NL cannot dock [39,40]. The NL docking involves NL strand β9 and the motor domain strand β0 forming a cover-neck bundle (CNB) [41] and when β0 and β9 are in proximity the CNB formation can take place.

(iii) The MT-bound head of undocked NL has a high binding energy with the detached ADP-head (denoted by E_{I1}), whereas the MT-bound head of docked NL has a weak binding energy with the detached ADP-head (denoted by E_{I2}).

Based on the above pieces of evidence or arguments, a forward stepping of the dimer and unbinding from weak affinity states at saturating ATP is schematically shown in Fig. 1. We begin with both heads in ADP.Pi state binding strongly to MT (Fig. 1a). The trailing head with the forward NL orientation has a much larger Pi-release rate than the leading head with the backward NL orientation (see next section). After Pi release in the trailing head, the ADP-head unbinds easily from site I by overcoming very weak affinity E_{w1} and then diffuses rapidly to the intermediate position relative to the MT-bound head, where the two heads have a high affinity (Fig. 1b). After NL docking, reducing greatly the interaction between the two heads (Fig. 1c), the detached ADP-head diffuses rapidly to the forward site III and binds to site III with affinity E_{w2} (Fig. 1d). Stimulated by MT, ADP is released, followed immediately by ATP binding and then ATP hydrolysis (Fig. 1e). From Fig. 1c, the detached ADP-head can also diffuses rapidly to the backward site I by overcoming the NL-docking energy E_{NL} and binds to site I with affinity E_{w2} (noting that after Pi release the affinity of the ADP-head to the local site changes rapidly from E_{w1} to E_{w2}), followed by ADP release, ATP binding and ATP hydrolysis (Fig. 1a). In Fig. 1b, Pi release can also occur occasionally in the MT-bound head before its NL docking takes place (Fig. 1f). Then, the dimer can unbind easily from MT by overcoming the very weak affinity E_{w1} during the period before the affinity of the MT-bound ADP-head for the local site II changes from E_{w1} to E_{w2} (called Period I). In Fig. 1d, Pi release can also occur occasionally in the trailing head before ADP release in the leading head (Fig. 1g). Then, the dimer can also unbind from MT by overcoming the weak affinity E_{w2} during the period before ADP release from the MT-bound head (called Period II). If the dimer has not unbound from MT until ADP release (Fig. 1h), the system becomes the same as Fig. 1b except that the dimer took a forward step.

Note that in Fig. 1 we show only the transitions related to the stepping and the weak affinity states of the motor to MT, which occur after Pi release in the trailing head. Other transitions can also occur. For example, Pi release can also occur occasionally in the leading head, giving a futile chemomechanical coupling cycle or a backward stepping.

Based on the model, the equations to describe the mechanical stepping and unbinding from the weak affinity states are presented in our previous works [31], with which the mechanical step of a kinesin head following Pi release relative to the other MT-bound head and the unbinding of the dimer from MT can be calculated using stochastic Runge–Kutta algorithm. Then, we can simulate processive movement and unbinding time of the dimer by also considering continuous ATPase activities, which can be simulated using Monte-Carlo algorithm [31]. From a simulated trace of the displacement of the center of mass of the dimer versus time, the total displacement (or run length) of the trace

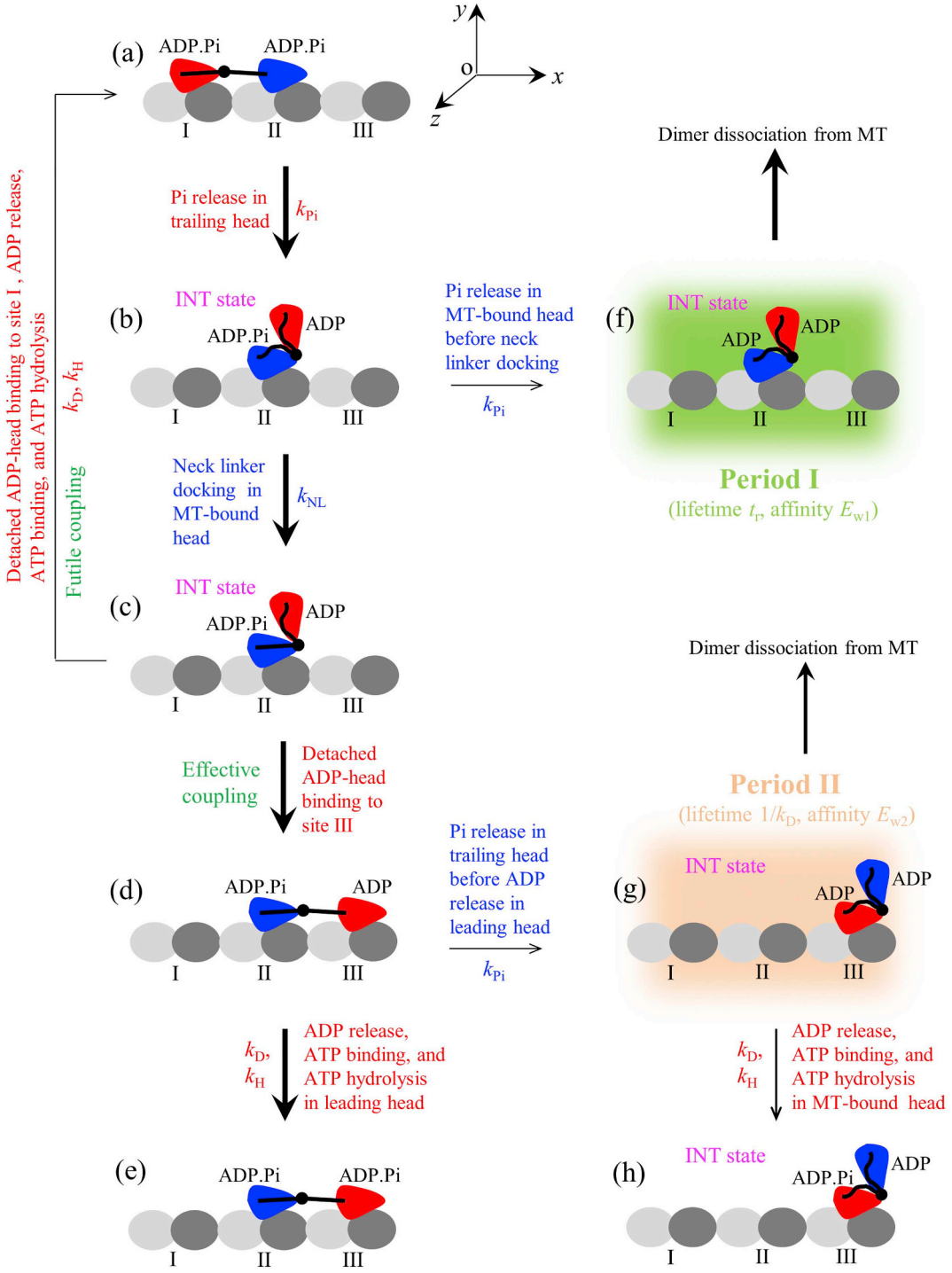

Fig. 1. Model of a forward stepping of kinesin motor on an MT filament and the occurrence of the weak affinity state after Pi release in the trailing head at saturating ATP concentration. The thickness of the arrow represents the magnitude of the transition rate or probability under no load. (a) Both heads in ADP.Pi state bind strongly to two successive binding sites on the MT filament. The trailing head with the forward NL orientation has a much larger Pi-release rate than the leading head with the backward NL orientation. (b) Upon Pi release taking place in the trailing head, due to very weak affinity E_{w1} between the ADP-head and the local site I, the trailing ADP-head unbinds from site I and then diffuses rapidly to the intermediate position relative to the MT-bound head, where the two heads have a high affinity. (c) NL docking in the MT-bound head takes place, weakening greatly the interaction between the two heads. (d) The thermal noise drives the tethered ADP-head to diffuse rapidly to the nearest site III and then bind to the site. (e) Stimulated by MT ADP is released from the leading lead, followed immediately by ATP binding and then ATP hydrolysis. (f) From (b) Pi release can also occur occasionally in the MT-bound head before its NL docking takes place. During the period before the affinity of the MT-bound ADP-head for the local site II changes from E_{w1} to E_{w2} (called Period I, shaded in green), the dimer can easily unbind from MT by overcoming the very weak affinity E_{w1} within time t_r. (g) From (d) Pi release can also occur occasionally in the trailing head before ADP release in the leading head. During the period before ADP release from the MT-bound head (called Period II, shaded in light red), the dimer has a large probability to unbind from MT by overcoming the weak affinity E_{w2}. (h) From (g) the dimer has not unbound from MT until ADP release, which is followed immediately by ATP binding and then ATP hydrolysis. (For interpretation of the references to colour in this figure legend, the reader is referred to the web version of this article.)

Table 1
Values of parameters for kinesin-1.

Parameter	Parameter description	Value	Reference
t_r	Lifetime of Period I	10 μs	[31,32]
E_{w1}	Weak affinity in Period I	$\leq 18k_BT$	[31,32]
E_{w2}	Weak affinity in Period II	$40k_BT$	[31,32]
E_{NL}	NL docking energy	$6k_BT$	[31,32]
k_{NL}	Rate constant of NL docking in ADP.Pi state	800 s^{-1}	[45]
k_H	Rate constant of ATP hydrolysis	350 s^{-1}	[5]
k_{Pi}	Rate constant of Pi release from head with forward NL orientation	140 s^{-1}	[46]
k_{Pi}/ρ	Rate constant of Pi release from head without forward NL orientation	$\rho = 30$	[17,18,31]
k_D	Rate constant of ADP release from MT-bound head	350 s^{-1}	[5,46]
ε_{s0}	Unbinding rate from the strong affinity state at $F = 0$	0.1 s^{-1}	fit to experiment [16]

can be obtained and the velocity of the trace can be calculated by dividing the total displacement by the unbinding time. The mean velocity and mean run length are calculated statistically using about 500 simulated traces.

2.2. The choice of parameter values

We take the similar parameter values to those we took before [31,32], which are described as follows. We take $t_r = 10$ μs, $E_{w1} \leq 18k_BT$, $E_{w2} = 40k_BT$ and $E_{NL} = 6k_BT$ (see Table 1). We take $E_{I1} > 40k_BT$ and $E_{I2} < 20k_BT$. We take $k_{NL} = 800$ s^{-1} in ADP.Pi state, $k_{NL} \leq 1$ s^{-1} in ATP state and $k_{NL} = 0$ in φ or ADP state (see Table 1). The rate constants of ATPase activity are taken to be independent of the force on the NL, as the available experimental evidence indicated [42]. Since we focus only on saturating ATP concentration in this work, the rate constant of ATP binding is not required. The rate constant of ATP hydrolysis is taken as $k_H = 350$ s^{-1} (see Table 1), independent of the NL orientation direction. The rate constant of Pi release (the rate-limiting step of ATPase activity) is dependent on the NL orientation direction, with the forward orientation having a much larger Pi-release rate, $k_{Pi}^{(T)} = k_{Pi} = 140$ s^{-1}, than the backward orientation, $k_{Pi}^{(L)} = k_{Pi}/\rho$, with $\rho = 30$ (see Table 1). In the intermediate state state, when the NL of the MT-bound head is stretched to a length $l_{NL} > 2.8$ nm by a forward load, the NL is considered to be in the forward orientation and thus the rate constant of Pi release is equal to k_{Pi}, while in other cases with the NL being not in the forward orientation the rate constant of Pi release is equal to k_{Pi}/ρ. The rate constant of ADP release from MT-bound head is taken as $k_D = 350$ s^{-1} (see Table 1). When ADP-head is detached from MT, without MT stimulation the ADP-release rate is zero.

3. Results and discussion

3.1. Unbinding from weak affinity states

As done in our previous works [31], in this section we do not consider the unbinding of the kinesin head in the strong affinity state, i.e., in φ or ATP or ADP.Pi state. This implies that only when both heads are simultaneously in ADP state the unbinding of kinesin dimer from MT is taken into account. As shown before [31], with consideration of unbinding only from the weak affinity states, the calculated results on force dependences of both velocity and run length are in quantitative agreement with the available single-molecule data (Fig. 2a and b). In this work, we define load F having positive value when its longitudinal component is along the backward direction and having negative value

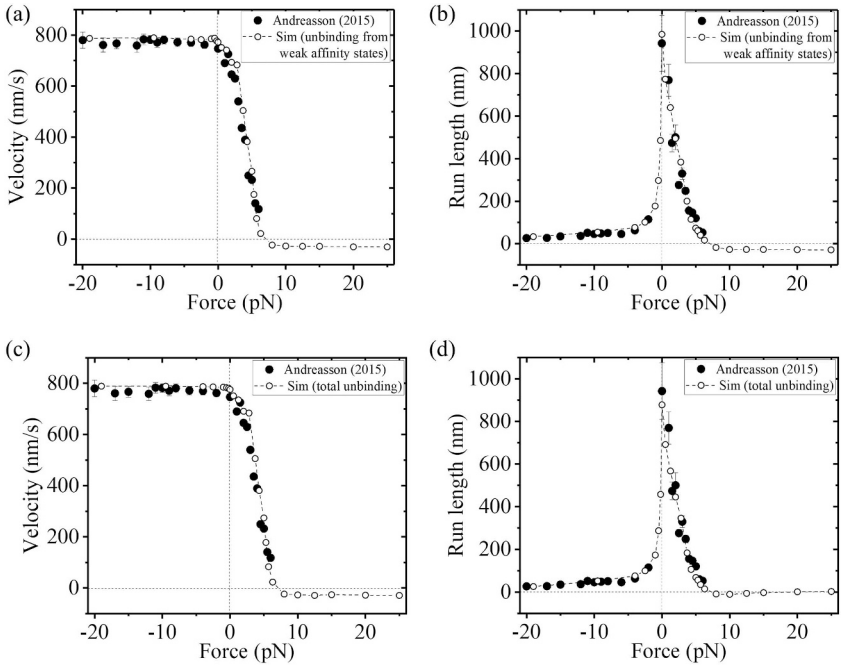

Fig. 2. Force dependences of velocity and run length of kinesin at saturating ATP concentration. Upper panels (a, b) show the results under the consideration that the kinesin can only unbind from MT in weak affinity states. Lower panels (c, d) show the results under the consideration that the kinesin can unbind from MT in both the weak and strong affinity states. Open symbols are calculated data and filled symbols are experimental data taken from Andreasson et al. [16]. (a, c) Velocity versus longitudinal component of the external force. (b, d) Run length versus longitudinal component of the external force.

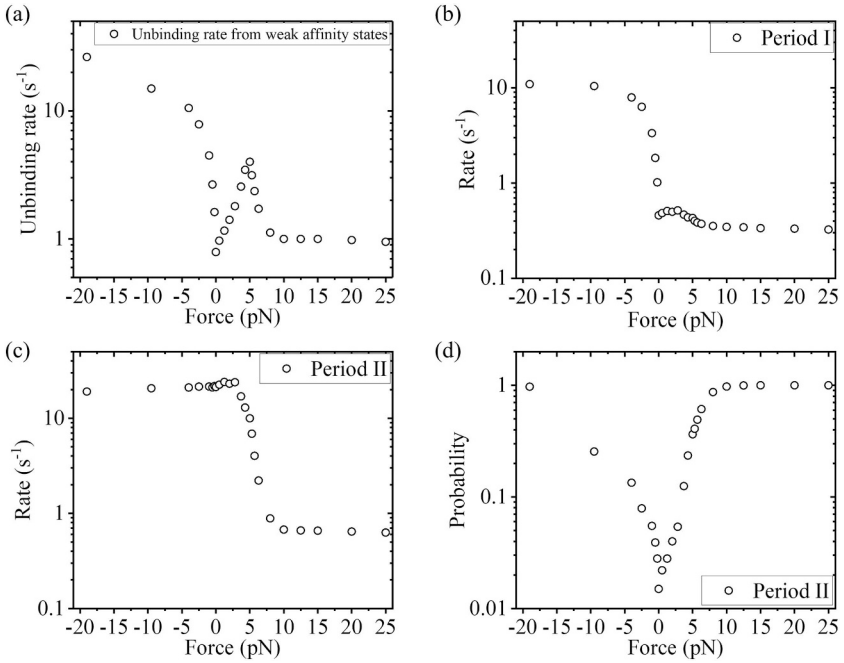

Fig. 3. Calculated results on unbinding of kinesin from MT at saturating ATP concentration under the consideration that the kinesin can only unbind from MT in weak affinity states. (a) Unbinding rate versus longitudinal component of the external force. (b) Occurrence rate of Period I versus longitudinal component of the external force. (c) Occurrence rate of Period II versus longitudinal component of the external force. (d) Probability of unbinding in Period II versus longitudinal component of the external force. Note that the vertical axes are plotted on a logarithmic scale.

when its longitudinal component is along the forward direction.

Here, we focus on the unbinding rate. As done in the experiments [16,19,43], the unbinding rate is defined as the inverse of the mean unbinding time, i.e., the mean time for the motor to bind to MT under a given load. In Fig. 3a we show the calculated results on the force dependence of the unbinding rate. From Fig. 3a it is seen that the unbinding rate increases rapidly with the increase in the magnitude of the forward load ($F < 0$) and then becomes increasing slowly with the further increase in the magnitude of the forward load. This can be expected from the curve of run length versus the forward load (Fig. 2b), showing that the run length decreases rapidly with the increase in the magnitude of the forward load ($F < 0$) and then becomes decreasing slowly with the further increase in the magnitude of the forward load, while the velocity is nearly unchanged with the variation of the forward load (Fig. 2a). Interestingly, from Fig. 3a we see that the unbinding rate increases exponentially with the increase of the backward load in the range of $0 \le F \le 5$ pN. The unbinding rate reaches the maximum value at about 5 pN. As the backward load increases further, the unbinding rate declines rapidly and then becomes saturated at high backward loads. This characteristic of the force dependence of unbinding rate can be understood as follows.

As discussed elsewhere [31,32], during the processive movement of a kinesin dimer on MT, the unbinding of the dimer from the weak affinity states takes place during two periods—Period I and Period II. Period I is after Pi release occurs in the MT-bound head and before the affinity of the MT-bound ADP-head for MT changes from E_{w1} to E_{w2} (shaded in green in Fig. 1). Period II is that the MT-bound head is in ADP state with its affinity for MT being E_{w2} (shaded in light red in Fig. 1). During Period I, since the affinity of the MT-bound head to MT is very weak, with a small value of E_{w1}, the head has a large probability to unbind from MT within time of t_r. During Period II, since ADP-head binds to MT weakly, with an affinity of E_{w2}, the head has a probability to unbind from MT before ADP release within a time of $1/k_D$ that is much longer than t_r. Consequently, the unbinding rate can be calculated by

$$\varepsilon_w = \sum_{i=1}^{2} \omega_i P_i \tag{1}$$

where ω_1 and ω_2 are the occurrence rates of Period I and Period II, respectively, during the processive movement of the dimer on MT, and P_1 and P_2 are the probabilities of dissociation occurring during Period I and Period II, respectively. With values of E_{w1} and t_r shown in Table 1, we have $P_1 \approx 1$ under any load. Hence, to see the origin of the characteristic of the force dependence of unbinding rate shown in Fig. 3a, we calculate rate ω_1 and ω_2 versus load, with the results being shown in Fig. 3b and c. The calculated results of probability P_2 versus load are shown in Fig. 3d (noting that the asymmetry of P_2 with respective to the forward and backward loads is due to the asymmetry of the weak potential between the ADP-head and MT-tubulin [31,32]). From Fig. 3b – d, it is noted that for $F < 0$ (the forward load), the unbinding of the motor is attributed mainly to that occurring in Period I, with ω_1 increasing rapidly with the increase in the magnitude of the forward load. The fact that the unbinding rate increases slowly with the further increase in magnitude of the forward load is attributed mainly to the increase of the probability P_2. For $F \ge 0$ (the backward load), the unbinding of the motor is attributed mainly to that occurring in Period II. In the range of $0 \le F < 5$ pN, the increase of the unbinding rate with the increase of F is attributed to the rapid increase of probability P_2, because ω_2 has a small change. When $F > 5$ pN, the rapid decrease of the unbinding rate is attributed to the rapid decrease of ω_2, because P_2 approaches its maximum of 1. Since the ATPase rate is nearly independent of F, the decline of ω_2 with F is due to the fact that the effective chemomechanical coupling ratio is reduced, which reduces the occurrence probability of Period II in one ATPase cycle (see Fig. 1). The saturation of the unbinding rate at large values of F is due to that both ω_2 and P_2 become saturated.

3.2. Unbinding from both weak and strong affinity states

Up to now, we have only considered the unbinding from the weak affinity state and have neglected the unbinding from the strong affinity state, i.e., the state with at least one head in ATP, ADP.Pi or φ state bound strongly to MT. In the small range of the external load, the consideration is reasonable. However, in the large external load, the unbinding from the strong affinity state should also be considered.

During the processive movement of the kinesin motor, the total period of the weak affinity states, which includes Period I and Period II, constitutes only a very small fraction of the whole period of one chemomechanical coupling cycle. In other words, in one chemomechanical coupling cycle the motors is almost always in the strong affinity state. Thus, for a good approximation, the unbinding time of the kinesin motor from the strong affinity state during its processive movement is simply equivalent to the time of a Brownian particle escaping from a potential well of large depth. For simplicity, we consider that the strong potential between the head and MT-tubulin is symmetrical with respect to the forward and backward loads. According to Kramers theory, the unbinding rate from the strong affinity state can be simply calculated by

$$\varepsilon_S = \varepsilon_{S0} \exp\left(\frac{|F|\ \delta}{k_B T}\right) \tag{2}$$

where ε_{S0} is the unbinding rate at $F = 0$ and δ is the interaction distance between the motor and MT-tubulin. To be consistent with the Debye length that is in the order of 1 nm in solution, we take $\delta = 1$ nm here. Therefore, the total unbinding rate of the motor can be calculated by

$$\varepsilon = \varepsilon_W + \varepsilon_S \tag{3}$$

where ε_W can be calculated by Eq. (1), with the results being shown in Fig. 3a.

With Eqs. (2) and (3), by adjusting $\varepsilon_{S0} = 0.1\ s^{-1}$ we obtain the total unbinding rate at $F = 25$ pN as $\varepsilon \approx 45\ s^{-1}$, which is close to the experimental data of Andreasson et al. [16]. Thus, we take $\varepsilon_{S0} = 0.1\ s^{-1}$ throughout our calculations (see Table 1). In Fig. 4 (dashed line) we show the results of ε_S versus F calculated with Eq. (2). The total unbinding rate is also shown in Fig. 4 (red circles), where for comparison the calculated data of the unbinding rate from the weak affinity states are reshown (blue circles). From Fig. 4 it is interesting to see that while the total unbinding rate under the forward load ($F < 0$) has the expected characteristic of slip bond, with the total unbinding rate increasing monotonically with the increase in the magnitude of the forward load, the total unbinding rate under the backward load ($F > 0$) shows counterintuitive characteristic of slip-catch-slip bond. The total unbinding rate increases firstly with the increase of the backward load. After reaching the maximum value, the total unbinding rate then decreases with the increase of the backward load. After the minimum value, the total unbinding rate then increases again with the increase of the backward load.

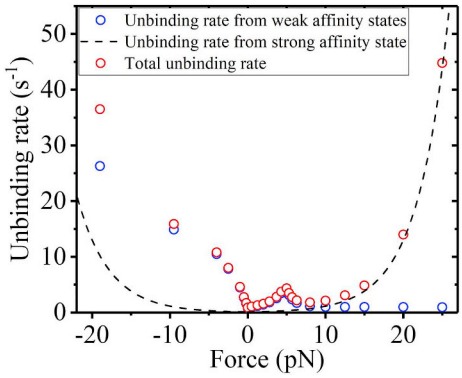

Fig. 4. Unbinding rate of kinesin from MT versus longitudinal component of the external force at saturating ATP concentration. Blue circles are the results under the consideration that the kinesin can only unbind from MT in weak affinity states. Dashed lines are the results under the consideration that the kinesin can only unbind from MT in the strong affinity state. Red circles are the results under the consideration that the kinesin can unbind from MT in both the weak and strong affinity states. (For interpretation of the references to colour in this figure legend, the reader is referred to the web version of this article.)

It is noted that since under no load the unbinding rate from the strong affinity state, $\varepsilon_{S0} = 0.1\ s^{-1}$, is much smaller than that from the weak affinity states (Fig. 3a), the inclusion of the unbinding from the strong affinity state has only a slight effect on the total unbinding rate in the small range of $|F| < 8$ pN (Fig. 4). Moreover, it is noted that the calculated results on the force dependences of velocity and run length by including the unbinding from the strong affinity state are also in good agreement with the available experimental data (Fig. 2c and d).

3.3. The calculated results of the force dependence of total unbinding rate are consistent with the available single-molecule data

Our calculated results show that the dependence of the total unbinding rate of kinesin from MT on the forward load ($F < 0$) exhibits the slip characteristic (left panel of Fig. 5a). This is consistent with the experimental data of Andreasson et al. [16] (right panel of Fig. 5a). Moreover, the calculated results show that the dependence of the total unbinding rate on the backward load ($F > 0$) exhibits the slip-catch-slip characteristic (left panel of Fig. 5a). Examining the experimental data of Andreasson et al. [16] (right panel of Fig. 5a), it is also noted that the unbinding rate increases firstly with the increase of the backward load in the range of $0 \le F \le 7$ pN (the experimental data can be fitted well with $\varepsilon = \varepsilon_0 \exp(F/F_d)$, where $\varepsilon_0 = 0.85\ s^{-1}$ and $F_d = 3.85$ pN, not shown here). The unbinding rate at $F \approx 10$ pN is smaller than that at $F \approx 7$ pN. After $F \approx 10$ pN the unbinding rate increases again with the increase of the backward load (the experimental data can be fitted well with $\varepsilon = \varepsilon_0 \exp(F/F_d)$, where $\varepsilon_0 = 0.96\ s^{-1}$ and $F_d = 6.5$ pN, not shown here). Thus, our calculated data and the experimental data of Andreasson et al. [16] under the backward loads are also consistent with each other.

Our calculated results of the total unbinding rate versus the backward load in the range of $0 \le F \le 15$ pN are also in agreement with the experimental data of Kunwar et al. [19], as shown in Fig. 5b. By fitting to the experimental data of Schnitzer et al. [44], Kunwar et al. [19] showed that in the range of $0 \le F < 5$ pN the dependence of the unbinding rate of kinesin from MT can be described well by $\varepsilon = \varepsilon_0 \exp(F/F_d)$, where $\varepsilon_0 = 1\ s^{-1}$ and $F_d = 3.2$ pN (dashed line in right panel of Fig. 5b). In the range of 5.6 pN $\le F \le$ 15 pN, Kunwar et al. [19] showed that their experimental data (dots in right panel of Fig. 5b) can be fitted with $\varepsilon = a + bF$, where $a = 1.07\ s^{-1}$ and $b = 0.186\ s^{-1}pN^{-1}$ (solid line in right panel of Fig. 5b). By comparison, our calculated data in the range of $0 \le F < 5$ pN can be fitted well with $\varepsilon = \varepsilon_0 \exp(F/F_d)$, where $\varepsilon_0 = 0.89\ s^{-1}$ and $F_d = 3.2$ pN (dashed line in left panel of Fig. 5b), and our calculated data in the range of 6 pN $\le F \le$ 15 pN (dots in the left panel of Fig. 1b) are also close to the corresponding experimental data of Kunwar et al. [19] (solid line in the left panel of Fig. 1b).

Our calculated results of the total unbinding rate versus the backward load in the small range of $0 \le F \le 5.5$ pN are also consistent with the experimental data of Coppin et al. [43], as shown in Fig. 5c. Both the calculated data (left panel) and experimental data (right panel) show that the unbinding rate increases exponentially with the increase of the backward load and after reaching the maximum value at about 5 pN the unbinding rate decreases with the further increase of the backward load.

Taken together, our studies and comparisons with the available experimental data from different research groups indicate confidently that the dependence of the total unbinding rate on the backward load shows the slip-catch-slip characteristic.

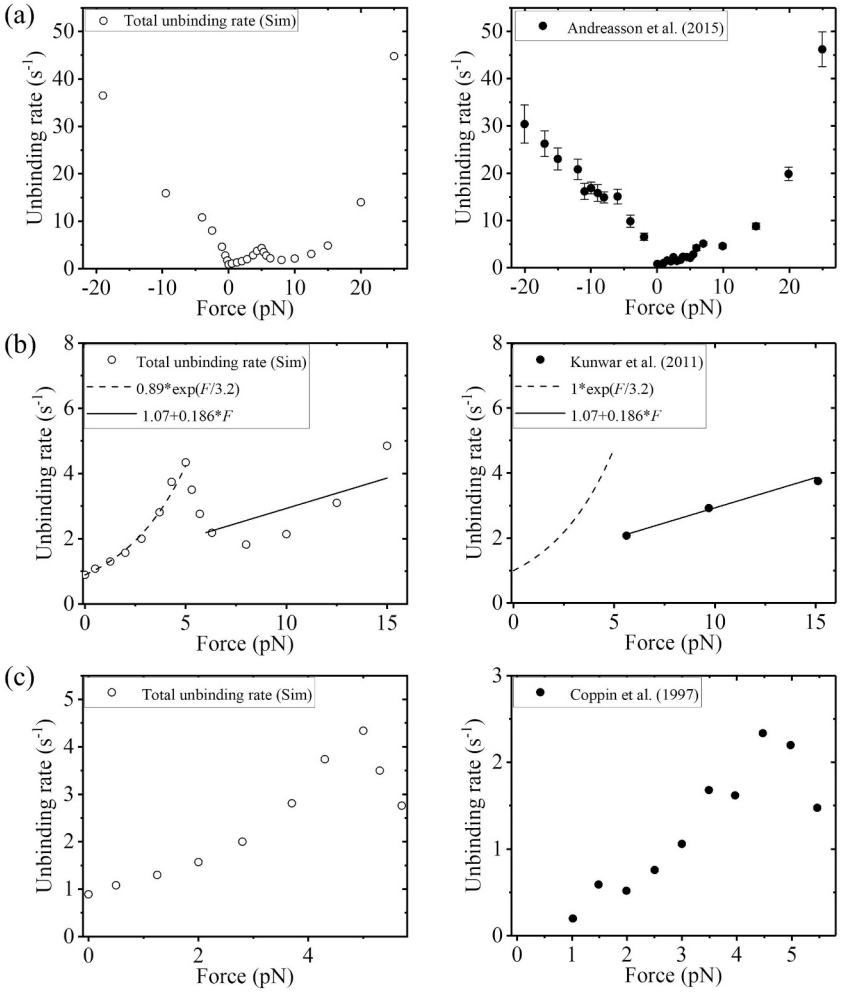

Fig. 5. Comparisons between calculated and available experimental data on force dependence of the unbinding rate. Left and right panels are the calculated and experimental data, respectively.

4. Concluding remarks

We study computationally the force dependence of the unbinding rate of the kinesin motor during its processive movement on MT. Our results show that the curve of the unbinding rate versus the external force exhibits three distinct regions (see left panel of Fig. 5a). In the range of about – 20 pN $< F <$ 0, the unbinding rate is mainly attributed to the unbinding occurring during Period I of the weak affinity state. In the range of about 0 $< F <$ 8 pN, the unbinding rate ε is mainly attributed to the unbinding occurring during Period II of the weak affinity state. In the range of about $F >$ 8 pN, the unbinding rate is mainly attributed to the unbinding occurring during the period of the strong binding state. Furthermore, our calculations and comparisons with the available experimental data indicate that the dependence of the total unbinding rate on the backward load shows the characteristic of slip-catch-slip bond. The mechanism of the slip-catch-slip bond is revealed.

In addition, it is noted interestingly that when the unbinding from the strong affinity state is negligible, the unbinding rate under the backward load shows the characteristic of slip-catch bond (Fig. 3a). This curve of the unbinding rate versus backward load (Fig. 3a) is similar to the experimental one for dynein motor measured by Kunwar et al. [19].

Acknowledgments

This work was supported by the National Natural Science Foundation of China (Grant No. 11775301) and National Key R&D Program of China (2016YFA0301500).

References

[1] R.D. Vale, T.S. Reese, M.P. Sheetz, Identification of a novel force-generating protein, kinesin, involved in microtubule-based motility, Cell 42 (1985) 39–50.
[2] F. Kozielski, S. Sack, A. Marx, M. Thormählen, E. Schönbrunn, V. Biou, A. Thompson, E.M. Mandelkow, E. Mandelkow, The crystal structure of Dimeric Kinesin and implications for microtubule-dependent motility, Cell 91 (1997) 985–994.
[3] M. Kikkawa, The role of microtubules in processive kinesin movement, Trends Cell Biol. 18 (2008) 128–135.
[4] B. Gigant, W. Wang, B. Dreier, Q. Jiang, L. Pecqueur, A. Plückthun, C. Wang, M. Knossow, Structure of a kinesin–tubulin complex and implications for kinesin motility, Nature Structural &Amp; Molecular Biology 20 (2013) 1001.
[5] R.A. Cross, The kinetic mechanism of kinesin, Trends Biochem. Sci. 29 (2004) 301–309.
[6] C.L. Asbury, Kinesin: world's tiniest biped, Curr. Opin. Cell Biol. 17 (2005) 89–97.
[7] R.D. Vale, R.A. Milligan, The way things move: looking under the Hood of molecular motor proteins, Science 288 (2000) 88.
[8] A. Yildiz, P.R. Selvin, Kinesin: walking, crawling or sliding along? Trends Cell Biol. 15 (2005) 112–120.
[9] A.B. Kolomeisky, M.E. Fisher, Molecular motors: a theorist's perspective, Annu. Rev. Phys. Chem. 58 (2007) 675–695.

[10] P. Xie, Mechanism of processive movement of monomeric and dimeric kinesin molecules, Int. J. Biol. Sci. 6 (2010) 665–674.
[11] N. Hirokawa, Kinesin and dynein superfamily proteins and the mechanism of organelle transport, Science 279 (1998) 519.
[12] D. Chowdhury, Stochastic mechano-chemical kinetics of molecular motors: a multidisciplinary enterprise from a physicist's perspective, Phys. Rep. 529 (2013) 1–197.
[13] K. Visscher, M.J. Schnitzer, S.M. Block, Single kinesin molecules studied with a molecular force clamp, Nature 400 (1999) 184–189.
[14] N.J. Carter, R.A. Cross, Mechanics of the kinesin step, Nature 435 (2005) 308–312.
[15] M. Nishiyama, H. Higuchi, T. Yanagida, Chemomechanical coupling of the forward and backward steps of single kinesin molecules, Nat. Cell Biol. 4 (2002) 790–797.
[16] J.O.L. Andreasson, B. Milic, G.-Y. Chen, N.R. Guydosh, W.O. Hancock, S.M. Block, Examining kinesin processivity within a general gating framework, eLife 4 (2015) e07403.
[17] P. Xie, H. Chen, A non-tight chemomechanical coupling model for force-dependence of movement dynamics of molecular motors, Phys. Chem. Chem. Phys. 20 (2018) 4752–4759.
[18] P. Xie, S.-K. Guo, H. Chen, ATP-concentration- and force-dependent Chemomechanical coupling of Kinesin molecular motors, J. Chem. Inf. Model. 59 (2019) 360–372.
[19] A. Kunwar, S.K. Tripathy, J. Xu, M.K. Mattson, P. Anand, R. Sigua, M. Vershinin, R.J. McKenney, C.C. Yu, A. Mogilner, S.P. Gross, Mechanical stochastic tug-of-war models cannot explain bidirectional lipid-droplet transport, Proc. Natl. Acad. Sci. 108 (2011) 18960–18965.
[20] F. Berger, C. Keller, S. Klumpp, R. Lipowsky, Distinct transport regimes for two elastically coupled molecular motors, Phys. Rev. Lett. 108 (2012) 208101.
[21] F. Berger, C. Keller, R. Lipowsky, S. Klumpp, Elastic coupling effects in cooperative transport by a pair of molecular motors, Cell. Mol. Bioeng. 6 (2013) 48–64.
[22] G. Arpağ, S. Shastry, William O. Hancock, E. Tüzel, Transport by populations of fast and slow Kinesins uncovers novel family-dependent motor characteristics important for in vivo function, Biophys. J. 107 (2014) 1896–1904.
[23] B.J.N. Reddy, S. Tripathy, M. Vershinin, M.E. Tanenbaum, J. Xu, M. Mattson-Hoss, K. Arabi, D. Chapman, T. Doolin, C. Hyeon, S.P. Gross, Heterogeneity in kinesin function, Traffic 18 (2017) 658–671.
[24] Y.-B. Fu, S.-K. Guo, P.-Y. Wang, P. Xie, Dynamics of cooperative cargo transport by two elastically coupled kinesin motors, Eur Phys J E 42 (2019) 41.
[25] G. Arpağ, S.R. Norris, S.I. Mousavi, V. Soppina, K.J. Verhey, W.O. Hancock, E. Tüzel, Motor dynamics underlying cargo transport by pairs of Kinesin-1 and Kinesin-3 motors, Biophys. J. 116 (2019) 1115–1126.
[26] A. Takshak, N. Mishra, A. Kulkarni, A. Kunwar, Effect of fuel concentration on cargo transport by a team of Kinesin motors, Physica A 467 (2017) 395–406.
[27] S. Bouzat, Models for microtubule cargo transport coupling the Langevin equation to stochastic stepping motor dynamics: caring about fluctuations, Phys. Rev. E 93 (2016) 012401.
[28] J.C. Dallon, C. Leduc, S. Etienne-Manneville, S. Portet, Stochastic modeling reveals how motor protein and filament properties affect intermediate filament transport, J. Theor. Biol. 464 (2019) 132–148.
[29] A. Kunwar, M. Vershinin, J. Xu, S.P. Gross, Stepping, strain gating, and an unexpected force-velocity curve for multiple-motor-based transport, Curr. Biol. 18 (2008) 1173–1183.
[30] S. Bouzat, F. Falo, The influence of direct motor-motor interaction in models for cargo transport by a single team of motors, Phys. Biol. 7 (2010) 046009.
[31] S.-K. Guo, X.-X. Shi, P.-Y. Wang, P. Xie, Processivity of dimeric kinesin-1 molecular motors, FEBS Open Bio 8 (2018) 1332–1351.
[32] S.-K. Guo, W.-C. Wang, P.-Y. Wang, P. Xie, Force dependence of velocity and run length of Kinesin-1, Kinesin-2 and Kinesin-5 family molecular motors, Molecules 24 (2019) 287.
[33] S. Chakrabarti, M. Hinczewski, D. Thirumalai, Phenomenological and microscopic theories for catch bonds, J. Struct. Biol. 197 (2017) 50–56.
[34] I.M.T.C. Crevel, A. Lockhart, R.A. Cross, Weak and strong states of Kinesin and ncd, J. Mol. Biol. 257 (1996) 66–76.
[35] H. Sosa, E.J.G. Peterman, W.E. Moerner, L.S.B. Goldstein, ADP-induced rocking of the kinesin motor domain revealed by single-molecule fluorescence polarization microscopy, Nat. Struct. Biol. 8 (2001) 540–544.
[36] R.A. Cross, Review: Mechanochemistry of the kinesin-1 ATPase, Biopolymers 105 (2016) 476–482.
[37] M. Morikawa, H. Yajima, R. Nitta, S. Inoue, T. Ogura, C. Sato, N. Hirokawa, X-ray and Cryo-EM structures reveal mutual conformational changes of Kinesin and GTP-state microtubules upon binding, EMBO J. 34 (2015) 1270.
[38] X.-X. Shi, Y.-B. Fu, S.-K. Guo, P.-Y. Wang, H. Chen, P. Xie, Investigating role of conformational changes of microtubule in regulating its binding affinity to kinesin by all-atom molecular dynamics simulation, Proteins 86 (2018) 1127–1139.
[39] S. Rice, A.W. Lin, D. Safer, C.L. Hart, N. Naber, B.O. Carragher, S.M. Cain, E. Pechatnikova, E.M. Wilson-Kubalek, M. Whittaker, E. Pate, R. Cooke, E.W. Taylor, R.A. Milligan, R.D. Vale, A structural change in the kinesin motor protein that drives motility, Nature 402 (1999) 778–784.
[40] A.B. Asenjo, Y. Weinberg, H. Sosa, Nucleotide binding and hydrolysis induces a disorder-order transition in the kinesin neck-linker region, Nat. Struct. Mol. Biol. 13 (2006) 648–654.
[41] A.S. Khalil, D.C. Appleyard, A.K. Labno, A. Georges, M. Karplus, A.M. Belcher, W. Hwang, M.J. Lang, Kinesin's cover-neck bundle folds forward to generate force, Proc. Natl. Acad. Sci. 105 (2008) 19247.
[42] A. Yildiz, M. Tomishige, A. Gennerich, R.D. Vale, Intramolecular strain coordinates Kinesin stepping behavior along microtubules, Cell 134 (2008) 1030–1041.
[43] C.M. Coppin, D.W. Pierce, L. Hsu, R.D. Vale, The load dependence of kinesin's mechanical cycle, Proc. Natl. Acad. Sci. 94 (1997) 8539.
[44] M.J. Schnitzer, K. Visscher, S.M. Block, Force production by single kinesin motors, Nat. Cell Biol. 2 (2000) 718–723.
[45] S.S. Rosenfeld, G.M. Jefferson, P.H. King, ATP reorients the neck linker of Kinesin in two sequential steps, J. Biol. Chem. 276 (2001) 40167–40174.
[46] S.P. Gilbert, M.L. Moyer, K.A. Johnson, Alternating site mechanism of the Kinesin ATPase, Biochemistry 37 (1998) 792–799.